7

Signal Processing Methods for Doppler Radar Heart Rate Monitoring

Anders Høst-Madsen, Nicolas Petrochilos, Olga Boric-Lubecke,
Victor M. Lubecke, Byung-Kwon Park, and Qin Zhou

A practical means for unobtrusive and ubiquitous detection and monitoring of heart and respiration activity from a distance could be a powerful tool for health care, emergency, and surveillance applications, yet remains a largely unrealized goal. Without the need for contact or subject preparation (special clothing, attachments, etc.), this could better extend health monitoring to the chronically ill in routine life, allow wellness monitoring for a large population without known predisposition for risk or harm, and provide alarm and data in emergencies. Such technology could also be used to detect lost or hidden subjects, to help assess emotional state, and to compliment more cumbersome measurements as pre-screening. Doppler radar remote sensing of vital signs has shown promise to this end, with proof of concept demonstrated for various applications. Unfortunately, this principle has not been developed to the level of practical application, mainly due to a lack of an effective way to isolate desired target motion from interference. However, by leveraging recent advances in signal processing and wireless communications technologies, this technique has the potential to transcend mere novelty and make a profound impact on health and welfare in society.

7.1 Introduction

Practical non-contact detection and monitoring of human cardiopulmonary activity could be a powerful tool for health care, emergency, military, and security applications. Doppler radar remote sensing of heart and respiration activity has shown promise toward this end, with proof of concept demonstrated for various applications [3, 12, 14]. By estimating the associated Doppler shift in a radio signal reflected by the body, cardiopulmonary-related movement can be discerned without physical contact. Through its non-invasive nature, this approach is well suited to applications where it is important to minimize disruption of the subject's activity, particularly where prolonged monitoring is needed. A robust Doppler radar system would be well suited

to collection of long-term heartbeat interval data for heart rate variability (HRV) diagnosis and prognosis [8]. Additional benefits of microwave Doppler radar include the versatile ability to function at a distance through clothing, walls, or debris. This allows the system to be applied both in medical health care scenarios, where some degree of subject cooperation can be assumed, and in emergency response or security applications, where subjects do not or cannot cooperate. Alternative techniques for long-term medical monitoring typically require direct contact (ECG and Holter monitors, piezoelectric sensors), while minimally invasive techniques tend to require very accurate control or placement (laser Doppler vibrometer), which might not always be possible or desirable. The use of infrared (IR) body heat sensors in search and rescue operations is limited due to poor IR propagation properties through walls, rubble, and weather. While Doppler radar offers distinct advantages, this approach has not been developed to the level of practical application, mainly because there has been no genuine effective way to isolate desired target motion from other motion and other targets. Fortunately, through the application of recent advances in wireless communications and signal processing technologies, Doppler cardiopulmonary radar now has the potential to transcend mere novelty and make a significant impact on health care and national security.

The use of Doppler radar was demonstrated for detection of respiratory rate in 1975 [10], and heart rate in 1979 [11], using commercially available waveguide X-band Doppler transceivers. Our recent work to implement this concept by leveraging telecommunications technology, includes the detection of heart and respiration signals with existing wireless terminals [14, 15], implementation of dedicated low-cost microwave Doppler radars [5–7], and development of related software for automated rate detection [13]. Doppler sensing with communications signals in the 800–2400 MHz range has been demonstrated with very promising results for both detection of surface and internal heart and respiration motion [14]. Higher frequency signals like those used for motion-controlled doors and traffic lights, in the 10 GHz range, also work well for detection of cardiopulmonary motion at the chest surface, even through clothing [1]. While reliable heart and respiration rate extraction can be performed for relatively still and isolated subjects [6], it is a major challenge to obtain useful data in the presence of random motion of the human target, radar, peripheral human subjects, and other moving objects. Many contact (such as ECG, EEG) and non-contact medical measurements (such as fMRI) also suffer from motion artifacts due to random motion of the subject during the measurements. Various DSP techniques are used to extract useful data from such measurements [19]. The problem of background noise has been a barrier to bringing Doppler vital signs sensing into practical, everyday applications. We propose to explore promising new solutions to this problem, taking advantage of recent developments in wireless communications. These have the potential to not only improve the robustness of Doppler radar sensing to practical levels, but to also make possible the gathering of additional

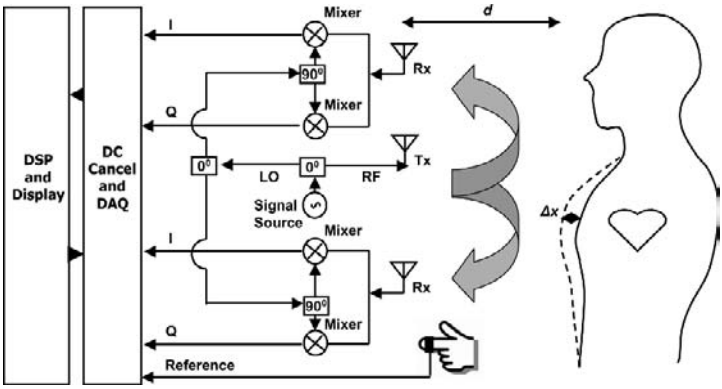

Fig. 7.1. A Doppler radar system with one transmit and two receive antennas. Each receive antenna is connected to a quadrature receiver chain to provide two orthonormal baseband signals (I and Q). DC components are eliminated via a dc canceller. Demodulated output results are compared with a wired finger pulse sensor reference

information, such as determining the number of subjects in a particular environment. The application of multiple input multiple output (MIMO) system techniques to provide robust Doppler radar heart signal detection as well as detection and count of multiple subjects will be discussed.

Multiple antennas can be used to detect multiple copies of the same signal with different phase information, with coherent combining used to provide a greatly improved estimate of desired Doppler motion. Figure 7.1 shows the block diagram of experimental set-up with one transmit and two receive antennas. Each receive antenna is connected to a quadrature receiver chain to provide two orthonormal baseband signals (I and Q). DC components are eliminated via a dc canceller. Demodulated output results are compared with a wired finger pulse sensor reference. When more than one target is in view, multiple transmitters and receivers providing multiple signal copies could be used to distinguish between the different sources of Doppler motion, and isolate the desired signal. We will first discuss demodulation methods for recovery of phase information in Doppler radar system, followed by signal processing methods for heart signal detection and estimation, and finally separation of multiple heartbeat signals.

7.2 Signal Model

In this section, we will discuss modeling of the signal. We assume a continuous wave (CW) radar system transmitting a single tone signal at frequency ω. The transmitted signal is

$$s(t) = \cos(\omega t + \phi(t)), \tag{7.1}$$

where $\phi(t)$ is phase noise in the oscillator.

This signal is reflected from a target at a nominal distance d, with a time-varying displacement given by $x(t)$. Suppose at first that the signal from the subject arrives from a single path. The received signal at the kth antenna is then

$$\begin{aligned} r_k(t) &= A_k \cos\left(\omega t - \frac{4\pi}{\lambda}(d + x(t) - k\tau) + \phi\left(t - \frac{2d}{c} - k\tau\right) + \varphi_0\right) + w_k(t) \\ \tau &= d_A \sin\alpha \end{aligned} \tag{7.2}$$

Here d_A is the inter-antenna spacing, α the angle of arrival, $w_k(t)$ the noise at the antenna, and A_k is the received amplitude at the kth antenna, which depends on the antenna pattern, e.g., if the antennas are omnidirectional, A_k is independent of k, and φ_0 some initial phase offset. To arrive at this, we have used some key properties of $x(t)$. First, $x(t)$ is slowly varying, so that $x(t - d/c - k\tau) \approx x(t)$. Second, $x(t)$ is small compared with d so that $\phi(t-(2d-x(t))/c-k\tau) \approx \phi(t-2d/c-k\tau)$. At the receiver, $r_k(t)$ is multiplied by $\cos(\omega t+\phi(t))$ and the phase-shifted signal $\sin(\omega t+\phi(t))$ and then lowpass filtered resulting in the complex signal

$$\begin{aligned} r_k(t) &= A_k \exp\left(\mathrm{j}\left(\frac{4\pi}{\lambda}(x(t) - k\tau) + \phi\left(t-\frac{2d}{c}-k\tau\right) - \phi(t) + \varphi\right)\right) + w_k(t) \\ &= C_k\, s_k(\tau)\, \exp\left(\mathrm{j}\Delta\phi_k(t)\right) \exp\left(\mathrm{j}\frac{4\pi}{\lambda}x(t)\right) + w_k(t) \end{aligned} \tag{7.3}$$

$$\begin{aligned} C_k &= A_k \mathrm{e}^{\mathrm{j}\varphi} \\ s_k(\tau) &= \mathrm{e}^{-\mathrm{j}\frac{4\pi}{\lambda}k\tau} \\ \Delta\phi_k(t) &= \phi\left(t - \frac{2d}{c} - k\tau\right) - \phi(t) \\ \varphi &= \frac{4\pi}{\lambda}d + \varphi_0 \end{aligned}$$

If $x(t)$ is small compared to λ and $\Delta\phi_k(t)$ is small, we can use a first order (i.e., linear) approximation for the complex exponential, so that

$$r_k(t) \approx C_k s_k(\tau) + C_k s_k(\tau)\mathrm{j}\frac{4\pi}{\lambda}x(t) + C_k s_k(\tau)\mathrm{j}\Delta\phi_k(t) + w_k(t) \tag{7.4}$$

So far we have assumed that the RF signal is only reflected by a single object, the subject of interest, and that only the vital sign signal is returned. However, there are multiple other reflections that must be taken into account. The signal is reflected by various stationary objects (e.g., walls) (and potentially moving objects, e.g., rustling leaves, although in many applications this is less likely). These reflections results in a dc-offset, as well as some additional noise. Thus, in most cases the dc of the signal contains no information and can be removed. This turns out to be of practical value as well. The signal due to the heartbeat is very small, and if the dc is not removed this gives dynamic range problems with the quantizer. Additionally, the signal reflected

off the body of the subject is also reflected by stationary objects, resulting in multipath. In that case the received signal is (after dc-removal)

$$r_k(t) = \exp\left(\mathrm{j}\frac{4\pi}{\lambda}x(t)\right)\sum_{i=1}^{M} C_{k,i}s_k(\tau_i)\exp\left(\mathrm{j}\Delta\phi_{k,i}(t)\right) + \tilde{w}_k(t) \tag{7.5}$$

where M is the number of multipath components. Each signal has its own signal strength $C_{k,i}$, angle of arrival (delay) $\tau_i = d_A \sin\alpha_i$, and phase noise contribution $\Delta\phi_{k,i}$. $x(t)$. The signal $x(t)$, of course, also experiences a different delay through the different paths, but this delay is insignificant relative to the bandwidth of $x(t)$. The non-linear model for multipath is rather complex, but if the linear model is valid, we get a simpler system model (again, after dc-removal)

$$\begin{aligned} r_k(t) &\approx x(t)\sum_{i=1}^{M} C_{k,i}s_k(\tau_i)j\frac{4\pi}{\lambda} + (\tilde{w})_k(t) \\ &= v_k x(t) + \tilde{w}_k(t), \end{aligned} \tag{7.6}$$

where v_k is a complex constant that summarizes all the factors affecting the signal at the nth antenna.

7.2.1 Physiological Signal Model

The signal displacement generated by the subject consists of respiration and heartbeat. The respiration is usually in the range 0.1–0.8 Hz and the heartbeat in the range 0.8–2 Hz. While the respiration is a stronger signal than the heartbeat, it is also more difficult to characterize and therefore to detect. In the current method, we therefore remove most of the respiration by high pass filtering. The heartbeat signal itself is a rather complicated signal. It is nearly periodic, but the period can vary from one beat to the next; this is called heart rate variability (HRV). HRV can be modeled as a random process [16] with strong periodicity. We consider the filtered received signal: bandpass filtered with a pass band of 0.8–2 Hz so that only the fundamental frequency of the heartbeat is received. The resulting signal is modeled as

$$s(t) = (A + \alpha(t))\cos(\omega t + \theta(t) + \theta_0). \tag{7.7}$$

The amplitude variations $\alpha(t)$ and $\theta(t)$ are zero mean random processes modeling the HRV. Notice that this is the same kind of model used in [22] but that the frequency ω is unknown here. Dealing directly with the model (7.7) for signal processing is complicated, since it is a non-linear function of a random process $\theta(t)$ that is not completely characterized. We therefore must use some approximation for $\theta(t)$. As $\theta(t)$ is rapidly varying (the time between heartbeats can vary 10% from one heartbeat to the next), a linear approximation

is not appropriate. Instead, we will use a piecewise constant approximation of $\varphi(t)$ (and $\alpha(t)$) so that

$$s(t) = A_i \cos(\omega t + \theta_i), \quad t \in [(i-1)T_0, iT_0], \tag{7.8}$$

where T_0 is some suitably chosen interval that can be optimized for performance, and A_i and φ_i are modeled as deterministic, unknown constants.

7.3 Single Person Signal Processing

7.3.1 Demodulation

Each antenna has two output signals, for a total of $2K$ signals. In a single person system, the first step is to combine these $2K$ signal into a single signal that best possible represents the heartbeat, a step we will call demodulation. The purpose is both graphical display of the signal (i.e., similar to the usual ECG signal), and to use in further signal processing. However, it should be noticed that the demodulated signal is not necessarily a sufficient statistic, so better performance can be obtained from using the $2K$ direct signals; this is in essence using the full MIMO advantage. However, using a single signal can considerably simplify signal processing.

There are two methods for demodulation. The first is *linear demodulation.* A linear demodulator is of the form

$$\hat{x}[n] = \sum_{k=1}^{K} a_k \Re(r_k[n]) + b_k \Im(r_k[n]) = \mathbf{d}^{\mathrm{T}} \mathbf{r}[n] \tag{7.9}$$

where $r_k[n]$ is the sampled version of $r_k(t)$, $\mathbf{d} = [\, a_1 \; b_1 \; \ldots \; a_K \; b_K \,]^T$, and $\mathbf{r}[n] = [\, \Re(r_1[n]) \; \Im(r_1[n]) \; \ldots \; \Re(r_K[n]) \; \Im(r_K[n]) \,]^{\mathrm{T}}$. As criterion for performance we will use mean square error (MSE)

$$\min_{\mathbf{d}} E\left[(\hat{x}[n] - x[n])^2\right]. \tag{7.10}$$

However, it can also be proven that the minimum MSE (MMSE) solution maximizes the signal-to-noise ration (SNR) at the output. In [23] we have proved that the optimum demodulator is projection onto the eigenvector corresponding to the maximum eigenvalue of the covariance matrix. This result is not surprising if the linear model (7.6) is assumed, but [23] shows it is also true for the non-linear model (without multipath).

The second method for demodulation is non-linear demodulation. This is mainly relevant for a single antenna, although non-linear modulation outputs from multiple antennas could be combined. So, assume a single antenna and let $r[n] = r_1[n]$ Clearly, from the model (7.5) the optimum non-linear demodulator is given by

$$\hat{x}[n] = \mathrm{Arg}(r[n] - c)\frac{\lambda}{4\pi}. \tag{7.11}$$

Here, c is unknown dc offset of the signal. So, to implement this estimator c needs to be known, or estimated.

It is easy to see that, given c, the ML estimator of the remaining parameters is

$$\hat{x}(c)[n] = \mathrm{Arg}(r[n] - c)\frac{\lambda}{4\pi}, \tag{7.12}$$

$$\hat{A}(c) = \frac{1}{N}\sum_{n=0}^{N-1} \Re\left\{(r[n] - c)\exp\left(-\mathrm{j}\frac{4\pi}{\lambda}\hat{x}(c)[n]\right)\right\}. \tag{7.13}$$

The estimation problem for c can now be stated as:

$$\hat{c} = \arg\min_{c\in\mathbb{R}} d(c) \tag{7.14}$$

$$d(c) = \sum_{n=0}^{N-1} \left|r[n] - \hat{A}(c)\exp(\mathrm{j}\hat{x}(c)[n]) - c\right|^2. \tag{7.15}$$

Unfortunately, a closed form expression for c does not exist, and the MLE is difficult to find numerically. In [17] we have developed a heuristic estimator for k, which is almost as good as the MLE for reasonable MSE.

The data in [17] shows that linear and non-linear demodulation is almost equivalent at low frequencies, such as the 2.4 GHz we use for experiments, but at higher frequencies, non-linear demodulation is better.

7.3.2 Detection of Heartbeat and Estimation of Heart Rate

In this section, we consider how to estimate the heart rate from the demodulated wireless signal and how to detect if a heartbeat is present. The signal after demodulation is still a very noisy signal. It does not have the well-defined peaks known from ECG signals, and methods from ECG signal processing therefore cannot be directly applied. We will first derive the maximum likelihood estimator (MLE) based on the model (7.8) for the heart rate, and corresponding to this the generalized likelihood ratio test (GLRT).

MLE Based on Demodulated Data

Consider estimation of average heart rate from the demodulated data. In that case the data is real, and we have a model

$$x[n] = s[n] + w[n], \tag{7.16}$$

where $w[n]$ is identically distributed zero mean real Gaussian noise with unknown variance σ^2. We assume the model (7.8), where $T_0 = NT$. We consider a *window* of data of length MN and divide this into M subwindows

of length N. We can then write the received signal $s_m[n]$ during the mth subwindow as

$$s_m[n] = A_m \cos(\omega n + \theta_m) = a_m \cos(\omega n) + b_m \sin(\omega n), \tag{7.17}$$

where the constant A_m includes all scaling due to body reflections, wireless propagation, demodulation, and heartbeat amplitude variations. For simplicity we use $\omega \in [0, \pi]$ for the discrete-time frequency. We can write the received signal during the mth subwindow as

$$x_m[n] = s_m[n] + w[n + mN]. \tag{7.18}$$

The joint density function for the observation vector is, under the assumption of white Gaussian noise

$$f_{\mathbf{\Phi}}(x) = \left(2\pi\sigma^2\right)^{-(MN/2)} \exp\left(-\frac{1}{2\sigma^2} \sum_{m=0}^{M-1} \sum_{n=0}^{N-1} \left(x_m[n] - s_m[n]\right)^2\right), \tag{7.19}$$

where $\mathbf{\Phi} = [\omega, \alpha_0, \ldots, \alpha_{M-1}, \beta_0, \ldots, \beta_{M-1}, \sigma^2]$ denotes the vector of unknown parameters. Define the square error γ^2 and γ_m^2

$$\gamma_m^2 = \sum_{n=0}^{N-1} \left(x_m[n] - s_m[n]\right)^2, \tag{7.20}$$

$$\gamma^2 = \sum_{m=0}^{M-1} \gamma_m^2. \tag{7.21}$$

To maximize the log-likelihood function is equivalent to minimize the square error γ^2, the summation of γ_m^2 over m. The maximization results in [23]

$$\hat{\omega} = \arg\max_{\omega} \frac{1}{M} \sum_{m=0}^{M-1} \left|X_m(\omega)\right|^2, \tag{7.22}$$

$$\hat{a}_m = \frac{1}{N} \Re\left\{X_m(\hat{\omega})\right\}, \tag{7.23}$$

$$\hat{b}_m = -\frac{1}{N} \Im\left\{X_m(\hat{\omega})\right\}, \tag{7.24}$$

$$\hat{\sigma}^2 = \frac{1}{MN} \left(\sum_{m=0}^{M-1} \sum_{n=0}^{N-1} x_m^2[n] - \frac{N}{2} \sum_{m=0}^{M-1} \left|X_m(\hat{\omega})\right|^2\right). \tag{7.25}$$

We notice that the ML estimator of the frequency is obtained from the combination of the DTFTs in each interval. Each of these can be calculated using FFTs, so the complexity of the algorithm is low.

For detection of heartbeat, we consider H_1 the hypothesis that a heartbeat is present, and H_0 that no heartbeat is present. Since heartbeat frequency and other parameter are unknown, this is a composite hypothesis test. A general

method and in many cases optimum solution for this problem is the generalized likelihood ratio test (GLRT) detector [18]. The principle is to estimate the unknown parameters under each of the hypothesis using the MLE, and then calculating the resulting likelihood ratio. Above, we have estimated the parameters under the H_1 hypothesis. Under the H_0 hypothesis, we only need to estimate the noise variance:

$$\hat{\sigma}^2 = \frac{1}{MN} \sum_{m=0}^{M-1} \sum_{n=0}^{N-1} x_m^2[n], \tag{7.26}$$

$$f_{\mathbf{\Phi}}(x; H_0) = \left(2\pi\hat{\theta}_0^2\right)^{-(MN/2)} \exp\left\{-\frac{MN}{2}\right\}. \tag{7.27}$$

Now we can represent the generalized likelihood ratio for hypothesis H_1 and H_0 as

$$L_G(x) = \frac{f_{\mathbf{\Phi}}(x; H_1)}{f_{\mathbf{\Phi}}(x; H_0)} = \left(\frac{\hat{\sigma}_1^2}{\hat{\sigma}_0^2}\right)^{-(MN/2)}. \tag{7.28}$$

MLE Estimator Based on Direct Data

As mentioned, the demodulated data does not constitute a sufficient statistic. We therefore consider ML estimation directly from the received data. Thus, we utilize more directly the MIMO advantage. As for the demodulated case, we divide the data into M windows of length N samples. The received signal at the kth antenna during the mth window can then be written as

$$z_{k,m}[n] = s_{k,m}[n] + w_{k,m}[n] = x_{k,m}[n] + jy_{k,m}[n], \tag{7.29}$$

where $(x_{k,m}[n], y_{k,m}[n])$ is the received I and Q data, and $w_{k,m}[n]$ is a sequence of independent, identically distributed zero mean circular complex Gaussian noise with unknown variance σ^2. Let $A_{k,m}$ and $B_{k,m}$ denote the magnitudes for the I and Q channel data for the kth antenna. We can write these as:

$$A_{k,m} = C_{k,m}\cos(\psi_k), \tag{7.30}$$

$$B_{k,m} = C_{k,m}\cos(\psi_k). \tag{7.31}$$

In the multipath model, it is most reasonable to assume that the ψ_k is independent between antennas. We can now write the received signal as

$$x_{k,m}[n] = A_{k,m}\cos(\omega t_{m,n} + \theta_m) + \Re\{w_{k,m}[n]\} \tag{7.32}$$

$$= \cos(\psi_k)\left(C_{k,m}\cos(\theta_m)\cos(\omega t_{m,n})\right. \tag{7.33}$$

$$\left. - C_{k,m}\sin(\theta_m)\sin(\omega t_{m,n})\right) + \Re\{w_{k,m}[n]\},$$

$$y_{k,m}[n] = A_{k,m}\cos(\omega t_{m,n} + \theta_m) + \Im\{w_{k,m}[n]\} \tag{7.34}$$

$$= \sin(\psi_k)\left(C_{k,m}\cos(\theta_m)\cos(\omega t_{m,n})\right. \tag{7.35}$$

$$\left. - C_{k,m}\sin(\theta_m)\sin(\omega t_{m,n})\right) + \Im\{w_{k,m}[n]\}. \tag{7.36}$$

It can be noticed here that ψ_k depends only on k while θ_m depends only on m. This is the most accurate model, but it seems impossible to get explicit expressions for the MLE estimator. We therefore consider two cases. First, we assume that ψ_k also depends on m. It can then be proven [23] that we get the following explicit solution:

$$\hat{\omega} = \arg\max_{\omega} \sum_{m=1}^{M} \left(\frac{1}{N} \sum_{k=1}^{K} |X_{k,m}(\omega)|^2 + |Y_{k,m}(\omega)|^2 + \frac{1}{N} \sqrt{g_m^2 + 4f_m^2} \right), \tag{7.37}$$

$$\hat{\sigma}^2 = \sum_{m=1}^{M} \left(\sum_{k=1}^{K} \sum_{n=0}^{N-1} x_{k,m}^2[n] + \sum_{k=1}^{K} \sum_{n=0}^{N-1} y_{k,m}^2[n] - \frac{1}{N} \sum_{k=1}^{K} |X_{k,m}(\hat{\omega})|^2 + |Y_{k,m}(\hat{\omega})|^2 - \frac{1}{N} \sqrt{g_m^2 + 4f_m^2} \right), \tag{7.38}$$

where

$$f_m = \sum_{k=1}^{K} \Re\{X_{k,m}(\omega)\} \Im\{X_{k,m}(\omega)\} + \Re\{Y_{k,m}(\omega)\} \Im\{Y_{k,m}(\omega)\}, \tag{7.39}$$

$$g_m = \sum_{k=1}^{K} \Re\{X_{k,m}(\omega)\}^2 + \Im\{X_{k,m}(\omega)\}^2 - \Re\{Y_{k,m}(\omega)\}^2 - \Im\{Y_{k,m}(\omega)\}^2. \tag{7.40}$$

The estimate of σ^2 can then be used in (7.28) to get the GLRT for this case.

Second, we assume that θ_m depends also on k. It can then be proved [23] that we get the following explicit solution:

$$\begin{aligned}
\hat{\omega} &= \arg\max_{\omega} \sum_{k=1}^{K} \Big(\|X_k(\omega)\|^2 + \|Y_k(\omega)\|^2 \\
&\quad + \sqrt{\left(\|X_k(\omega)\|^2 - \|Y_k(\omega)\|^2 \right)^2 + 4\Re\{X_k(\omega) Y_k(\omega)^*\}^2} \Big), \\
\sigma^2 &= \sum_{k=1}^{K} \gamma_k, \\
\gamma_k^2 &= \sum_{m=0}^{M-1} \sum_{n=0}^{N-1} x_{k,m}^2[n] + \sum_{m=0}^{M-1} \sum_{n=0}^{N-1} y_{k,m}^2[n], \\
&\quad - \frac{1}{N} \|X_k(\omega)\|^2 - \frac{1}{N} \|Y_k(\omega)\|^2, \\
&\quad - \frac{1}{N} \sqrt{\left(\|X_k(\omega)\|^2 - \|Y_k(\omega)\|^2 \right)^2 + 4\Re\{X_k(\omega) Y_k(\omega)^*\}^2},
\end{aligned} \tag{7.41}$$

where

$$\|X_k(\omega)\|^2 = \sum_{m=0}^{M-1} |X_{k,m}(\omega)|^2,$$
$$\|Y_k(\omega)\|^2 = \sum_{m=0}^{M-1} |Y_{k,m}(\omega)|^2,$$
$$X_k(\omega)Y_k(\omega)^* = \sum_{m=0}^{M-1} X_{k,m}Y_{k,m}(\omega)^*. \tag{7.42}$$

Again, the estimate of σ^2 can then be used in (7.28) to get the GLRT for this case.

What should be noticed is that although the solutions look complex, they are expressed as simple combinations of discrete time Fourier transforms, and therefore they can be calculated extremely fast using FFTs.

Figures 7.2 and 7.3 show the detection performance of the detectors in the form of ROCs (receiver operating characteristic) based on measured data for a number of subjects. Figure 7.2 compares the detector based on demodulated data ((7.25) and (7.28)) with one based on direct data ((7.41) and (7.28)); the figure confirms that using direct data is more efficient. Figure 7.3 compares the performance of the direct data detector for various sizes of windows and subwindows.

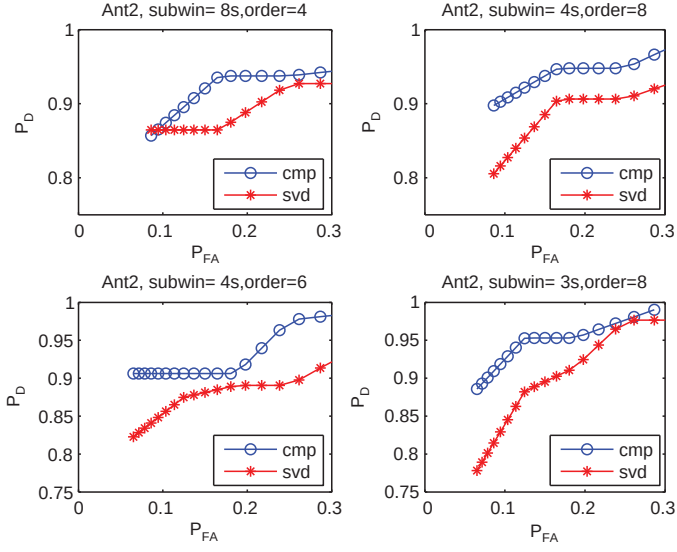

Fig. 7.2. ROC curves for the GLRT either based on demodulated data (SVD) or direct data (CMP)

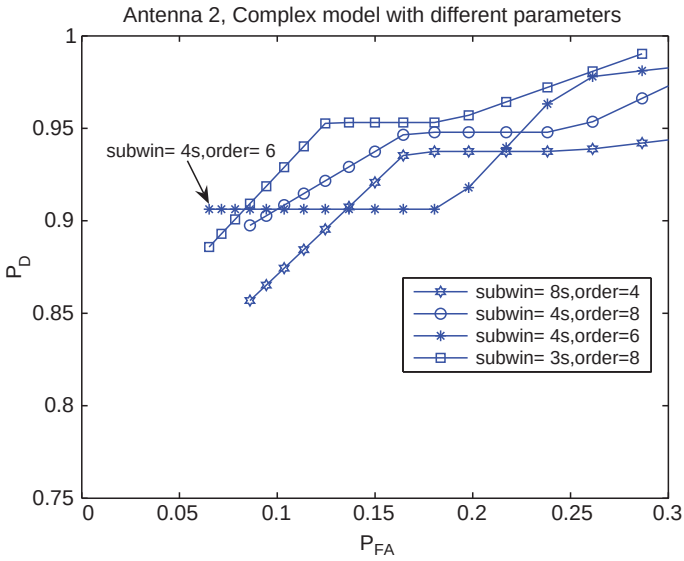

Fig. 7.3. Performance of the GLRT for direct data with different parameters

7.4 Multiple People Signal Processing

Consider the signal model (7.6). If there are d multiple sources, they add up linearly, resulting in

$$r_k(t) = \sum_{j=1}^{d} v_{k,j} x_j(t) + \tilde{w}_k(t) \tag{7.43}$$

In the sampled version, this can be written as the classical instantaneous linear model:

$$\mathbf{r}[n] = \mathbf{M}\ \mathbf{x}[n] + \mathbf{w}[n].$$

As the data is not known, nor the mixing matrix, blind source separation (BSS) methods are the natural choice. Note also that (1) the noise power is of the same magnitude or higher than the signal power, (2) the received IQ signal is complex, but the sources $s[n]$ are real, so we apply real BSS, and we work on:

$$\mathbf{y}[n] = \begin{bmatrix} \Re(\mathbf{r}[n]) \\ \Im(\mathbf{r}[n]) \end{bmatrix} = \begin{bmatrix} \Re(\mathbf{M}) \\ \Im(\mathbf{M}) \end{bmatrix} \mathbf{x}[n] + \begin{bmatrix} \Re(\mathbf{w}[n]) \\ \Im(\mathbf{w}[n]) \end{bmatrix},$$
$$\mathbf{y}[n] = \overline{\mathbf{M}}\mathbf{x}[n] + \overline{\mathbf{w}}[n], \tag{7.44}$$

where the size of the received signal is multiplied by two, thus allowing twice as many independent beamformers.

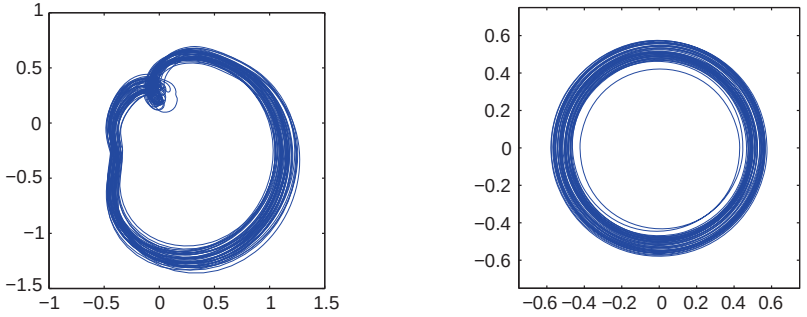

Fig. 7.4. Analytical representation of a finger pulse sensor signal after bandpass filtering in the range 0.03–30 Hz. (**a**) Full version, (**b**) Filtered version

The aim of multiple people signal processing is now to separate the multiple sources. Once they are separated, the single person signal processing from Sect. 7.3 can be utilized.

7.4.1 Heartbeat Signal

As a model for the heartbeat, we consider (7.7). Because of the phase variations $\theta(t)$ the signal is not strongly periodic. However, the amplitude $A+\alpha(t)$ is nearly constant, which means that $x(t)$ has an analytical representation which is almost a constant modulus signal. The analytical signal is obtained by adding the signal and the quadrature of its Hilbert transform [2].

Figure 7.4 shows the analytical signal of an ECG signal from, and its lowpass filtered version. The almost circular trajectory indicates that indeed the heartbeat signals are nearly constant modulus, and that after lowpass filtering, this property shows up even stronger.

In real-world applications, there might be many sources, but we are only interested in those that are heartbeat and/or respiration signals. We therefore need to use specific characteristics of these signals. One possibility is to use the signal that is quasi-periodic, as we used in the single person detector in Sect. 7.3. However, the signal is not very periodic, and we therefore believe that the constant modulus property is a stronger indicator. For this reason, we focus on BSS methods that use the constant modulus property.

7.4.2 Algorithm

Our algorithm is based on three steps:

(α) Use a band-pass filter over the range [0.75;2] Hz.
(β) Generate the analytic version of our signal by taking it and then adding its Hilbert Transform, $\mathcal{H}\{r(t)\}$, in quadrature:

$$r_a(t) = r(t) + \jmath\mathcal{H}\{r(t)\},$$

(γ) Use the ACMA algorithm on the data [21]. ACMA is a BSS algorithm that search for the beamformers $\mathbf{w}_i$, such that the estimated sources $\hat{x}_i = \mathbf{w}^H \mathbf{r}$ are constant-modulus: $|\hat{x}_i| \approx 1$.

Step α removes the heartbeat harmonics, the respiration and the low frequency interferences.

Doing these pre-processing steps insures that each source produces a *rank-one only matrix* and is constant-modulus, so that the assumptions needed by ACMA are respected.

The choice of the separation algorithm follows the next reasoning: RACMA [20] is then not applicable in our case, since at the end of step β, the sources are complex. ACMA [21] is the logical choice as it needs less samples than any HOS-based method, as ACI [4] or EFICA [9], is computationally faster, and our data is constant-modulus.

7.4.3 Results

As we do not have enough measurements with two subjects to draw statistically sound performance evaluations of our algorithm, we have to recourse to semi-synthesized and full simulations in this section.

We compare our method, PP-ACMA, to either RACMA, ICA, or EFICA. The later algorithms do not need the pre-processing to function, but we also evaluate EFICA with the pre-processed data in order to have a comparison that is fair to ACMA.

Simulations

To have better insight on the algorithm behavior, we conduct now the evaluation over fully simulated data, i.e., the heartbeat source signal are now generated by the method proposed in [16] with different average rate (so different subjects). Note that we can tune the signal noise ratio (SNR), the incoming average heart rate and time integration, and therefore fully explore the limits of the algorithms. Once the separation algorithm has delivered output signals, they are used to estimate the heart rate. The separation is declared a success if both measured hearbeats are within 0.08 Hz of their true values, and the output SINR is above 3 dB, otherwise it is a failure. We also compare to EFICA, which is either applied to the direct data or to the pre-processed data.

First, we consider two sources with an SNR of −5 dB, and an integration time of 6 s (so 120 samples). Figure 7.5 presents the success rate of the PP-ACMA, ICA, EFICA directly on data (denoted EFICA,R), and EFICA on the pre-processed data (denoted EFICA,C). We note that even two sources with the same average heart rate, due to the difference in HRV, the separation is still possible up to 50% of the cases with ACMA. In the other cases, ICA and EFICA (R) behaves also quite well, but not with a perfect 100% as the ACMA. Notice also that the pre-processed methods cannot work outside the frequency

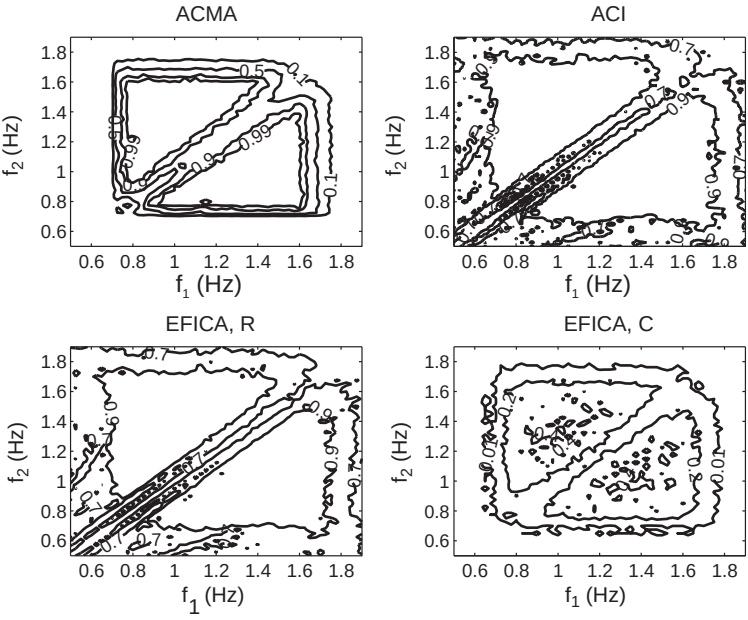

Fig. 7.5. Success rate of the algorithms as a function of average rate of the heartbeat

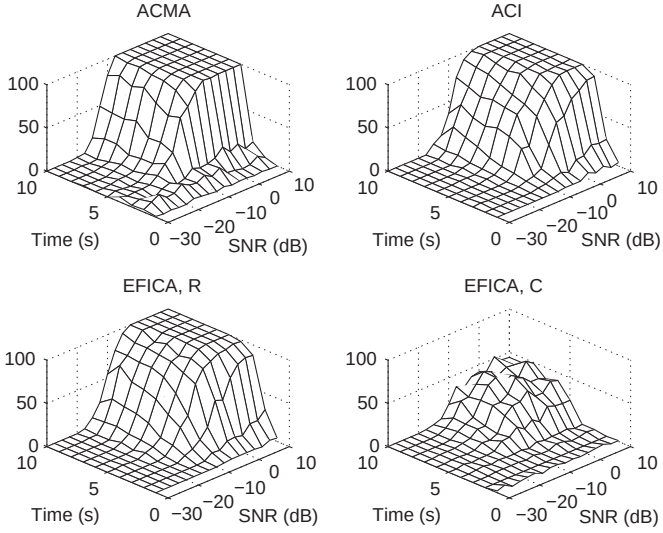

Fig. 7.6. Success rate of the algorithms as a function of SNR and the integration time

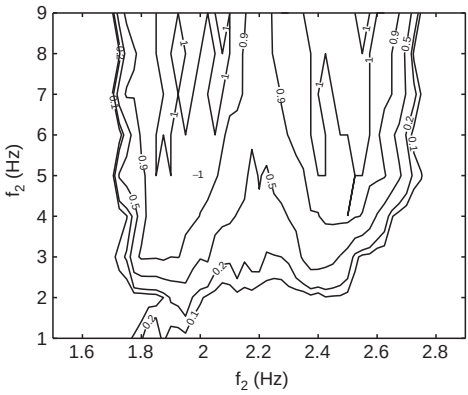

Fig. 7.7. Success rate of the PP-ACMA as a function of average rate of the second heartbeat and the integration time

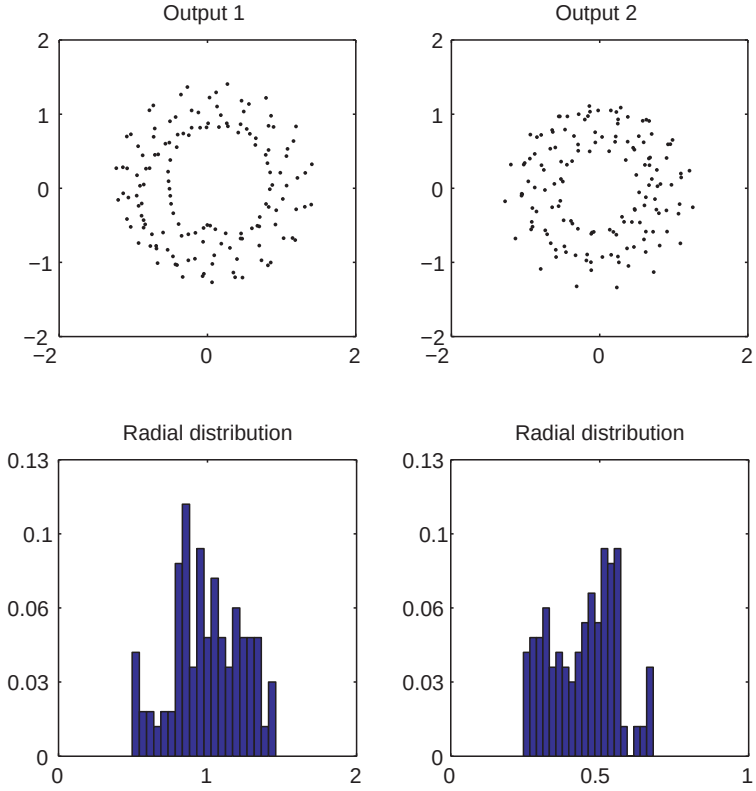

Fig. 7.8. Radial distribution of the two channels after separation with ACMA

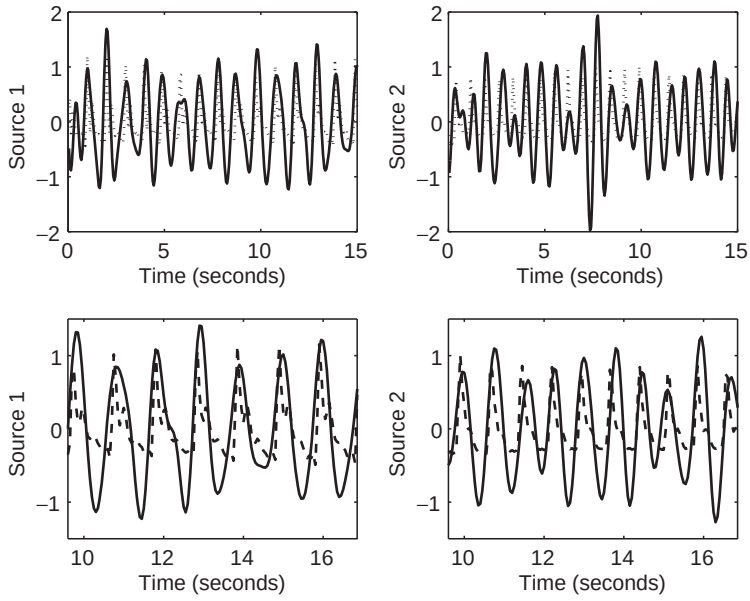

Fig. 7.9. The two separated sources in the time domain. The *solid curve* shows the reference measurements

range of the filters, but the frequency limits have been chosen according to reasonable heartbeat rate. Finally, we note that EFICA-C is not reliable in any case, this is due to the loss of diversity in the signal, which impairs the high-order statistics.

Next, we keep the frequencies fixed to 0.9 and 1.2 Hz, and we vary the SNR and the time of observation. We note in Fig. 7.6 that thanks to the pre-processing gain, acceptable success rate can be obtained till -15 dB SNR for PP-ACMA, and that 4 s is a minimum integration time (approximately four cycles). While ACI and EFICA-R needs 5 dB more, but 3 s is already enough for them. This counter-intuitive result can be explained by the fact that we do not strictly compare the algorithm over the same signals: indeed, for the PP-ACMA, the signal has been amputated from most of its harmonics and its spectral diversity, that ICA and EFICA-R are still using. Next to it, in a real scenario, where the pre-processing is mandatory, note that EFICA-C under-performs severely.

From now, we just concentrate on our scheme for our specific applications. We keep the first average frequency at 1.1 Hz, and we vary the other average frequency as well the time of integration. From Fig. 7.7, we confirm that given enough times of integration it is possible to separate two sources with equal average rate, as for instance for $T = 9$ s, the success rate is above 60%.

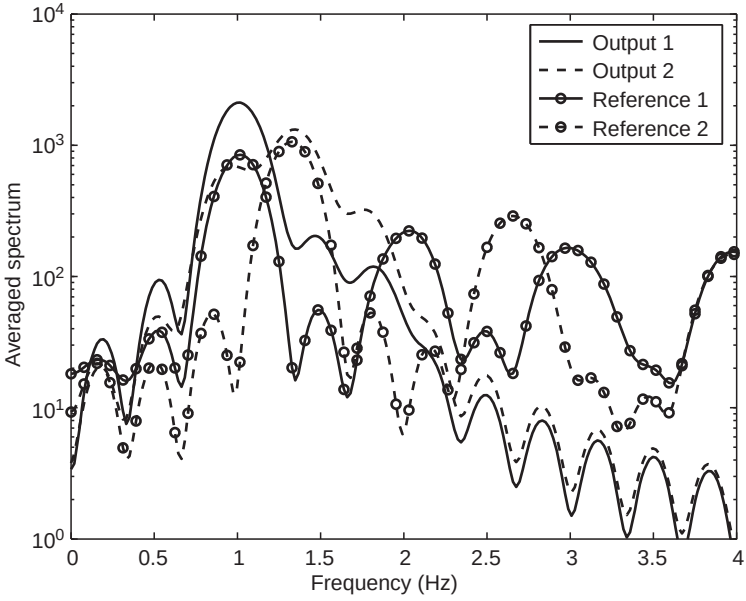

Fig. 7.10. The two separated sources in the frequency domain

Experimental Results

Finally, we will present some results from real measurements. The data is from a single experiment with two persons and two antennas. The ACMA algorithms was applied. Figure 7.8 shows the radial distribution after using ACMA. As can be seen, the CM property is well satisfied. Figures 7.9 and 7.10 show the two separated signals in the time domain, respectively, frequency domain. It can be seen that the two sources agree with the reference measurements, although there is some leakage from the stronger source to the weaker source.

7.5 Conclusion

In this chapter, we have outlined methods for signal processing of Doppler signals. The main problems we have focused on is detection of a signal and separation of multiple signals. We have outlined a number of methods for detection and separation and shown the efficacy on real signals. The key technology we considered was using multiple antenna transmitters and receivers. We first showed how this could be used for enhanced signal processing when a single person is present. We then showed how this could be used to monitor multiple persons.

Acknowledgement

This material is based upon work supported by the US National Science Foundation under Grant No. ECS0428975.

References

1. Boric-Lubecke, O., Ong, P.W., Lubecke, V.M.: 10 GHz Doppler radar sensing of respiration and heart movement. In: Proceedings of the IEEE 28th Annual Northeast Bioengineering Conference, pp. 55–56 (2002)
2. Bracewell, R.: The Fourier Transform and Its Applications, 3rd edn. McGraw-Hill, New York (1999)
3. Chen, K.M., Mirsa, D., Wang, H., Chuang, H.R., Postow, E.: An X-band microwave life detection system. IEEE Transactions on Biomedical Engineering **33**, 697–70 (1986)
4. Comon, P.: Independent component analysis, a new concept? Signal Processing, Special issue on Higher-Order Statistics **36**(3), 287–314 (1994)
5. Droitcour, A., Boric-Lubecke, O., Lubecke, V.M., Lin, J.: 0.25 μm CMOS and biCMOS single chip direct conversion Doppler radars for remote sensing of vital signs. In: IEEE ISSCC Digest of Technical Papers, pp. 348–349 (2002)
6. Droitcour, A.D., Boric-Lubecke, O., Lubecke, V.M., Lin, J., Kovacs, G.T.A.: Range correlation effect on ISM band I/Q CMOS radar for non-contact sensing of vital signs. In: IEEE MTT-S IMS2003 Digest, vol. 3, pp. 1945–1948 (2003)
7. Droitcour, A.D., Lubecke, V.M., Lin, J., Boric-Lubecke, O.: A microwave radio for Doppler radar sensing of vital signs. In: IEEE MTT-S IMS2001 Digest, vol. 1, pp. 175–178 (2001)
8. Hilton, M.F., Bates, R.A., Godfrey, K.R., et al.: Evaluation of frequency and time-frequency spectral analysis of heart rate variability as a diagnostic marker of the sleep apnea syndrome. Medical and Biological Engineering and Computing **37**(6), 760–769 (1999)
9. Koldovsk, Z., Tichavsk, P., Oja, E.: Dfficient variant of algorithm fastica for independent component analysis attaining the Cramer–Rao lower bound. IEEE Transactions on Neural Networks **17**(5), 1265–1277 (2006)
10. Lin, J.C.: Non-invasive microwave measurement of respiration. Proceedings of IEEE **63**, 1530 (1975)
11. Lin, J.C.: Microwave apexcardiography. IEEE Transactions MTT **27**, 618–620 (1979)
12. Lin, J.C.: Microwave sensing of physiological movement and volume change: A review. Bioelectromagnetics **13**, 557–565 (1992)
13. Lohman, B.B., Boric-Lubecke, O., Lubecke, V.M., Ong, P.W., Sondhi, M.M.: A digital signal processor for Doppler radar sensing of vital signs. In: 23rd Annual International Conference of the IEEE Engineering in Medicine and Biology Society (2001)
14. Lubecke, V., Boric-Lubecke, O., Awater, G., Ong, P.W., Gammel, P., Yan, R.H., Lin, J.C.: Remote sensing of vital signs with telecommunications signals. In: World Congress on Medical Physics and Biomedical Engineering (2000)

15. Lubecke, V., Boric-Lubecke, O., Beck, E.: A compact low-cost add-on module for Doppler radar sensing of vital signs using a wireless communications terminal. In: IEEE MTT-S International Microwave Symposium (2002)
16. McSharry, P.E., Clifford, G.D., Tarassenko, L., Smith, L.: A dynamical model for generating synthetic electrocardiogram signals. IEEE Transactions Biomedical Engineering **50**, 289–294 (2003)
17. Park, B.K., Vergara, A., Boric-Lubecke, O., Lubecke, V., Høst-Madsen, A.: Center tracking quadrature demodulation for a Doppler radar motion detector. IEEE Transactions on Microwave Theory and Techniques (2007). Submitted. Available at http://www.ee.hawaii.edu/∼madsen/papers/index.html
18. Poor, H.V.: An Introduction to Signal Detection and Estimation. Springer, Berlin Heidelberg New York (1994)
19. Thakor, N.V., Zhu, Y.S.: Application of adaptive filtering to ECG analysis: Noise cancellation and arrhythmia detection. IEEE Transactions on Biomedical Enginering **38**, 785–794 (1991)
20. van der Veen, A.: Analytical method for blind binary signal separation. IEEE Transactions on Signal Processing **45**(4), 1078–1082 (1997)
21. van der Veen, A., Paulraj, A.: An analytical constant modulus algorithm. IEEE Transactions on Signal Processing **44**(5), 1136–1155 (1996)
22. Veeravalli, V., Poor, H.: Quadratic detection of signals with drifting phase. Journal of the Acoustic Society of America **89**, 811–819 (1991)
23. Zhou, Q., Petrochilos, N., Høst-Madsen, A., Boric-Lubecke, O., Lubecke, V.: Detection and monitoring of heartbeat using Doppler radar. IEEE Transactions on Signal Processing (2007). Submitted. Available at http://www.ee.hawaii.edu/∼madsen/papers/index.html